ITERATIVE SPACE-TIME ADAPTIVE PROCESSING

J. Li X. Zhu P. Stoica M. Rangaswamy

J. Li and X. Zhu are with the Department of Electrical and Computer Engineering, University of Florida, Gainesville, FL 32611-6130, USA
P. Stoica is with the Department of Information Technology, Uppsala University, Uppsala, Sweden
M. Rangaswamy is with the Air Force Research Laboratory Sensors Directorate, Hanscom AFB, MA01731

ABSTRACT

To reduce the need of secondary data and/or accurate prior knowledge of the clutter statistics in space-time adaptive processing (STAP), we present herein *a user parameter-free and secondary data-free* fully automatic weighted least squares based iterative adaptive approach (IAA) to angle-Doppler imaging for airborne surveillance radar systems.

1. INTRODUCTION

In conventional STAP, the clutter-and-noise covariance matrix of the range bin of current interest, let us call it $\mathbf{R}_{\text{CN}}$, is estimated from secondary data (presumed to be target free and homogeneous). Given, say N adjacent range bins (snapshots) denoted as $\{\mathbf{z}(n)\}_{n=1}^{N}$, $\mathbf{R}_{\text{CN}}$ is estimated by means of the well-known formula to compute the sample covariance matrix (see, e.g., [1, 2]):

$$\hat{\mathbf{R}}_{\text{CN}} = \frac{1}{N}\sum_{n=1}^{N}\mathbf{z}(n)\mathbf{z}^{*}(n), \tag{1}$$

where $(\cdot)^{*}$ denotes the conjugate transpose. However, frequently the dimension of $\mathbf{R}_{\text{CN}}$ (denoted by M in what follows) is larger than N due to the inhomogeneous nature of the clutter and the fact that the adjacent range bins are not necessarily target free. The result is that $\hat{\mathbf{R}}_{\text{CN}}$ is, more often than not, a poor estimate of $\mathbf{R}_{\text{CN}}$.

Getting high quality secondary data has turned out to be a challenging problem. As a result, knowledge-aided STAP has been attracting attention lately (see, e.g., [2–4] and the references therein). However, getting accurate prior knowledge of the clutter statistics can be rather expensive. And using inaccurate prior knowledge can degrade rather than improve the STAP performance (see, e.g., [4]).

To reduce the need of secondary data and/or accurate prior knowledge of the clutter statistics, many approaches have been considered in the literature (see, e.g., [5] - [9]). The joint-domain localized approach proposed in [5] requires using the delay-and-sum (DAS) (i.e., least-squares or matched filter) type of approaches to transform the data into the angle-Doppler domain. It is well-known, however, that such data-independent approaches suffer from broad mainbeam (smearing) and high sidelobe level (leakage) problems that can degrade the target detection performance significantly. For the case of ULAs and constant PRFs, one can form multiple "snapshots" by taking sub-apertures in both space and time (see, e.g., [6]). However, this is done at the cost of reduced resolution. Moreover, in practice, the arrays many not be uniform and linear. The parametric approaches considered in [8,9] model the clutter and noise as a vector autoregressive (VAR) random process. However, the parametric approaches may be sensitive to model errors, which may occur in the presence of spatial and temporal decorrelation due to intrinsic clutter motion. The global matched filter approach considered in [7] can be used to form angle-Doppler image of both clutter and targets for each range bin using only the data from that range bin (primary data). The approach belongs to the class of sparse signal representation methods. However, these sparse signal representation algorithms usually require large computation times and the tuning of one or more user parameters, which may limit their practicality.

We present herein a user parameter-free and secondary data-free fully automatic angle-Doppler imaging approach for STAP by means of a weighted least-squares based iterative adaptive approach (IAA) [10]. IAA is a robust nonparametric adaptive algorithm that can work with few or even a single snapshot, arbitrary array geometries, and random time samples. In the IAA-based STAP, we apply IAA to form a high-resolution angle-Doppler image of both clutter and targets for each range bin of interest using the primary data only. The high resolution angle-Doppler images formed by IAA can be exploited further to identify clutter inhomogeneity and strong clutter discretes, check the accuracy of the prior knowledge, and combine with localized detection approaches as well as other target tracking approaches for target detection.

This work was supported in part by the Office of Naval Research (ONR) under Grant N00014-07-1-0293, the Army Research Office (ARO) under Grant No. W911NF-07-1-0450, the National Science Foundation (NSF) under Grant No. ECCS-0729727, and the Swedish Research Council (VR). Opinions, interpretations, conclusions, and recommendations are those of the authors and are not necessarily endorsed by the United States Government.

Report Documentation Page

Form Approved
OMB No. 0704-0188

1. REPORT DATE	2. REPORT TYPE	3. DATES COVERED
JAN 2009		**00-00-2009 to 00-00-2009**

4. TITLE AND SUBTITLE	5a. CONTRACT NUMBER
Iterative Space-Time Adaptive Processing	5b. GRANT NUMBER
	5c. PROGRAM ELEMENT NUMBER
6. AUTHOR(S)	5d. PROJECT NUMBER
	5e. TASK NUMBER
	5f. WORK UNIT NUMBER
7. PERFORMING ORGANIZATION NAME(S) AND ADDRESS(ES) **University of Florida,Department of Electrical and Computer Engineering,Gainesville,FL,32611-6130**	8. PERFORMING ORGANIZATION REPORT NUMBER
9. SPONSORING/MONITORING AGENCY NAME(S) AND ADDRESS(ES)	10. SPONSOR/MONITOR'S ACRONYM(S)
	11. SPONSOR/MONITOR'S REPORT NUMBER(S)

12. DISTRIBUTION/AVAILABILITY STATEMENT
Approved for public release; distribution unlimited

13. SUPPLEMENTARY NOTES
See also ADM002264. Presented at the IEEE Digital Signal Processing Workshop (13th) and Signal Processing Education Workshop (5th) Held in Marco Island, Florida on 4-7 January 2009. Sponsored by ONR.

14. ABSTRACT
To reduce the need of secondary data and/or accurate prior knowledge of the clutter statistics in space-time adaptive processing (STAP), we present herein a user parameter-free and secondary data-free fully automatic weighted least squares based iterative adaptive approach (IAA) to angle-Doppler imaging for airborne surveillance radar systems.

15. SUBJECT TERMS

16. SECURITY CLASSIFICATION OF:			17. LIMITATION OF ABSTRACT	18. NUMBER OF PAGES	19a. NAME OF RESPONSIBLE PERSON
a. REPORT	b. ABSTRACT	c. THIS PAGE			
unclassified	**unclassified**	**unclassified**	**Same as Report (SAR)**	**6**	

2. ANGLE-DOPPLER IMAGING VIA IAA

Assume that the radar system has L antennas and P pulses. Then $M = PL$. Within a coherent processing interval (CPI), we assume that echoes from I range bins are collected by the radar. For a fixed elevation angle, a target can be specified by its range index i, azimuth angle (or spatial frequency $\omega_{\rm S}$), and Doppler frequency $\omega_{\rm D}$. Its "nominal" space-time steering vector $\mathbf{a}(\omega_{\rm S}, \omega_{\rm D}) \in \mathbb{C}^{M\times 1}$ can be expressed as follows:

$$\mathbf{a}(\omega_{\rm S}, \omega_{\rm D}) = \tilde{\mathbf{a}}(\omega_{\rm D}) \otimes \bar{\mathbf{a}}(\omega_{\rm S}), \tag{2}$$

where $\otimes$ denotes the Kronecker matrix product. For the case of a ULA and a constant PRF, for example,

$$\bar{\mathbf{a}}(\omega_{\rm S}) = \left[\begin{array}{cccc} 1 & e^{j\omega_{\rm S}} & \cdots & e^{j(L-1)\omega_{\rm S}} \end{array}\right]^T, \tag{3}$$

and

$$\tilde{\mathbf{a}}(\omega_{\rm D}) = \left[\begin{array}{cccc} 1 & e^{j\omega_{\rm D}} & \cdots & e^{j(P-1)\omega_{\rm D}} \end{array}\right]^T, \tag{4}$$

where $(\cdot)^T$ denotes the transpose. However, IAA is equally applicable to the case of arbitrary array geometries and/or time-varying pulse repetition intervals.

For each ROI, we scan over both angle and Doppler dimensions to form its angle-Doppler image, i.e., to compute the two-dimensional power distribution of targets as well as clutter-and-noise, using the primary data only. For notational convenience, we drop below the dependence on the range bin index. Assume that the number of angular and Doppler scanning (grid) points are $\bar{K}$ and $\tilde{K}$, respectively, which determine the smoothness of the angle-Doppler image formed by IAA. Then the total number of scanning points is $K = \bar{K}\tilde{K}$. Let $\mathbf{P}$ be a diagonal matrix of dimension K with the powers of the scanning points on the diagonal. Given $\mathbf{P}$, we can construct the following IAA covariance matrix for the ROI:

$$\mathbf{R}_{\rm IAA} = \mathbf{APA}^*, \tag{5}$$

where $\mathbf{A} = [\mathbf{a}(\omega_{\rm S_1}, \omega_{\rm D_1}), \mathbf{a}(\omega_{\rm S_1}, \omega_{\rm D_2}), \cdots, \mathbf{a}(\omega_{\rm S_{\bar{K}}}, \omega_{\rm D_{\tilde{K}}})]$ is an $M \times K$ steering matrix. Given $\mathbf{R}_{\rm IAA}$ in (5) and also the primary data vector $\mathbf{y}$ for the ROI, an estimate of the power $P_{\bar{k}\tilde{k}}$, denoted as $\hat{P}_{\bar{k}\tilde{k}}$, at the scanning point $(\omega_{\rm S_{\bar{k}}}, \omega_{\rm D_{\tilde{k}}})$, can be computed as:

$$\hat{P}_{\bar{k}\tilde{k}} = \left| \frac{\mathbf{a}^*(\omega_{\rm S_{\bar{k}}}, \omega_{\rm D_{\tilde{k}}})\mathbf{R}_{\rm IAA}^{-1}\mathbf{y}}{\mathbf{a}^*(\omega_{\rm S_{\bar{k}}}, \omega_{\rm D_{\tilde{k}}})\mathbf{R}_{\rm IAA}^{-1}\mathbf{a}(\omega_{\rm S_{\bar{k}}}, \omega_{\rm D_{\tilde{k}}})} \right|^2, \tag{6}$$

where $P_{\bar{k}\tilde{k}}$ is a diagonal element of $\mathbf{P}$, and $|\cdot|$ denotes the absolute value. Since IAA requires $\mathbf{R}_{\rm IAA}$, which depends on the unknown powers, it must be implemented as an iterative approach. The initialization is done by the standard DAS beamformer, i.e., the so-called matched filter, where the signal power is determined in the same way as IAA except that $\mathbf{R}_{\rm IAA}$ in (6) is replaced by the identity matrix $\mathbf{I}$. The IAA algorithm is summarized in Table 1. The iterative process stops when a prescribed iteration number is achieved. This number is set to 10 in our simulations as we have observed no obvious performance improvement beyond 10 iterations. It is clear from the above discussions that the IAA-based angle-Doppler imaging approach is both user parameter-free and secondary data-free.

Table 1. The IAA algorithm

initialize $P_{\bar{k},\tilde{k}}(i) = \frac{1}{M^2}\left|\mathbf{a}^*(\omega_{\rm S_{\bar{k}}}, \omega_{\rm D_{\tilde{k}}})\mathbf{y}\right|^2$,
$\bar{k} = 1, \cdots, \bar{K}$, and $\tilde{k} = 1, \cdots, \tilde{K}$
repeat $\mathbf{R}_{\rm IAA} = \mathbf{APA}^*$
  for $\bar{k} = 1, \cdots, \bar{K}$
    for $\tilde{k} = 1, \cdots, \tilde{K}$
      $P_{\bar{k},\tilde{k}} = \left| \frac{\mathbf{a}^*(\omega_{\rm S_{\bar{k}}}, \omega_{\rm D_{\tilde{k}}})\mathbf{R}_{\rm IAA}^{-1}\mathbf{y}}{\mathbf{a}^*(\omega_{\rm S_{\bar{k}}}, \omega_{\rm D_{\tilde{k}}})\mathbf{R}_{\rm IAA}^{-1}\mathbf{a}(\omega_{\rm S_{\bar{k}}}, \omega_{\rm D_{\tilde{k}}})} \right|^2$
    end
  end
until a certain number of iterations is reached

The computationally complexity of IAA is on the order of $O(M^2K)$, where $K \gg M$ is the number of grid points in the angle-Doppler image. The computational complexity of IAA can be significantly reduced for the case of ULAs and constant PRFs by exploiting the Toeplitz-block-Toeoplitz structure of $\mathbf{R}_{\rm IAA}$ [11].

3. NUMERICAL EXAMPLES

3.1. Simulated Data

In our simulations, we employ the same parameters as those used to generate the KASSPER data [12] to simulate realistic inhomogeneous clutter. Consider an airborne radar system with $P = 32$ pulses and $L = 11$ spatial channels, yielding $M = PL = 352$ degrees-of-freedom (DOFs). The mainbeam of the radar is steered toward an azimuth angle of 195° measured clockwise from the true north and an elevation of -5° relative to the horizon. For each CPI, a total of $I = 1000$ range bins are sampled covering a range swath of interest from 35 km to 50 km. Since $\mathbf{R}_{\rm CN}$, $\hat{\mathbf{R}}_{\rm CN}$, and $\mathbf{R}_{\rm IAA}$ all vary with the range bin index i, in what follows, we will indicate explicitly the dependence of these covariance matrices on the range bin index for the sake of clarity. We generate the *clutter-and-noise* data for the ith range bin as:

$$\mathbf{e}_i = \mathbf{R}_{\rm CN}^{1/2}(i)\mathbf{v}_i, \quad i = 1, \cdots, I, \tag{7}$$

where $(\cdot)^{1/2}$ denotes a Hermitian square root of a matrix and $\{\mathbf{v}_i\} \in \mathbb{C}^{M\times 1}$ are independent and identically distributed (i.i.d.) circularly symmetric complex Gaussian random vectors with mean $\mathbf{0}$ and covariance matrix $\mathbf{I}$.

3.1.1. Angle-Doppler Imaging

Consider the angle-Doppler imaging performance in the presence of targets. We insert a total of $K_0 = 200$ targets spread

over the entire range-Doppler map at the azimuth angle of 195°. Each target is assumed to have a constant power σ_0^2, as shown in Figure 1, where the ground truth is denoted by "o". In our simulations, the targets have an average signal-to-clutter-and-noise ratio (SCNR) of -18.9 dB, where the average SCNR is defined as:

$$\frac{1}{K_0}\sum_{k=1}^{K_0}\frac{\mathrm{tr}\left[\sigma_0^2\mathbf{a}_0(\omega_{\mathrm{S}_0},\omega_{\mathrm{D}_k})\mathbf{a}_0^*(\omega_{\mathrm{S}_0},\omega_{\mathrm{D}_k})\right]}{\mathrm{tr}\left[\mathbf{R}_{\mathrm{CN}}(i_k)\right]}. \tag{8}$$

In (8), $\mathbf{a}_0(\omega_{\mathrm{S}_0},\omega_{\mathrm{D}_k})$ is the true steering vector corresponding to the fixed spatial frequency ω_{S_0} for the $195°$ azimuth angle and the Doppler frequency ω_{D_k} for the kth target at range bin i_k. The power estimate obtained from the received signal $\mathbf{y}_i$,

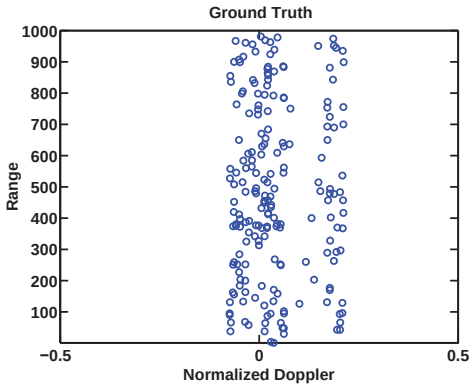

Fig. 1. Ground truth of targets.

which consists of both clutter-and-noise $\mathbf{e}_i$ and targets, at a given angle and Doppler pair $(\omega_{\mathrm{S}},\omega_{\mathrm{D}})$ is computed, similarly to (6), as follows:

$$\left|\frac{\mathbf{a}^*(\omega_{\mathrm{S}},\omega_{\mathrm{D}})\tilde{\mathbf{R}}^{-1}(i)\mathbf{y}_i}{\mathbf{a}^*(\omega_{\mathrm{S}},\omega_{\mathrm{D}})\tilde{\mathbf{R}}^{-1}(i)\mathbf{a}(\omega_{\mathrm{S}},\omega_{\mathrm{D}})}\right|^2. \tag{9}$$

We compare the performance achieved by using the covariance matrix $\mathbf{R}_{\mathrm{IAA}}(i)$ to those corresponding to various alternative covariance matrices, namely: the true clutter-and-noise covariance matrix $\mathbf{R}_{\mathrm{CN}}(i)$, the true target-clutter-and-noise covariance matrix $\mathbf{R}_{\mathrm{TCN}}(i)$, and an imprecise prior knowledge-based covariance matrix $\mathbf{R}_0(i)$. For the clairvoyant case of known $\mathbf{R}_{\mathrm{TCN}}(i)$, $\mathbf{R}_{\mathrm{TCN}}(i)$ is assumed to be:

$$\mathbf{R}_{\mathrm{TCN}}(i)=\mathbf{R}_{\mathrm{CN}}(i)+\sum_{k=1}^{K_0(i)}\sigma_0^2\mathbf{a}_0(\omega_{\mathrm{S}_0},\omega_{\mathrm{D}_k}(i))\mathbf{a}_0^*(\omega_{\mathrm{S}_0},\omega_{\mathrm{D}_k}(i)), \tag{10}$$

where $K_0(i)$ denotes the number of targets for the ith range bin and $\omega_{\mathrm{D}_k}(i)$ denotes the Doppler frequency of the kth target at the ith range bin. In our simulations, $\mathbf{R}_0(i)$ is constructed as a perturbed version of the true $\mathbf{R}_{\mathrm{CN}}(i)$ [4]:

$$\mathbf{R}_0(i)=\mathbf{R}_{\mathrm{CN}}(i)\odot\mathbf{t}_i\mathbf{t}_i^*, \tag{11}$$

where $\odot$ denotes the Hadamard matrix product, and $\mathbf{t}_i$ is a vector of i.i.d. complex Gaussian random variables with mean 1 and variance $\sigma_t^2=0.1$.

We now compare the angle-Doppler images formed with IAA and other methods for the ROI with range bin index $i=66$. Figures 2 and 3, respectively, are for the cases of without and with array steering vector errors. Figures 2(a) and 3(a) are obtained by using the true target-clutter-and-noise covariance matrix $\mathbf{R}_{\mathrm{TCN}}(i)$ in lieu of $\tilde{\mathbf{R}}(i)$ in (9). Note that in the absence of steering vector errors, the angle-Doppler image formed by using $\mathbf{R}_{\mathrm{TCN}}(i)$ is very sharp, with the clutter well focused along the diagonal ridge and the two moving targets clearly visible. In the presence of steering vector errors, however, the angle-Doppler image formed by using $\mathbf{R}_{\mathrm{TCN}}(i)$ is much worse, due to the well-known signal cancellation problems of standard Capon beamformer (SCB)[SCB corresponds to using $\mathbf{R}_{\mathrm{CN}}(i)$ in lieu of $\tilde{\mathbf{R}}(i)$ in (9)] [13].

Figures 2(b) and 3(b) are obtained by using the prior knowledge of the clutter-and-noise covariance matrix, $\mathbf{R}_0(i)$, which is a perturbed version of the true clutter-and-noise covariance matrix $\mathbf{R}_{\mathrm{CN}}(i)$. Note that the angle-Doppler images formed by using the wrong prior knowledge are rather smeared and are of poor quality. Figures 2(c) and 3(c) are obtained by using the true clutter-and-noise covariance matrix $\mathbf{R}_{\mathrm{CN}}(i)$. Note the obvious smearing caused by the presence of the moving targets. This result occurs because $\mathbf{R}_{\mathrm{CN}}(i)$ does not contain the target information and hence the adaptive processing is not adapted to the presence of targets. Therefore, the power estimation using $\mathbf{R}_{\mathrm{CN}}(i)$ in general is *not* optimal in any sense. (The only optimal case is when there is a single target at the range bin and the steering vector is pointed precisely at the target location.) Figures 2(d) and 3(d) are generated by using the DAS approach [i.e. using $\tilde{\mathbf{R}}(i)=\mathbf{I}$ in (9)]. Due to the smearing and leakage problems of DAS, the two moving targets are barely visible.

Figures 2(e) and 3(e) are obtained by using IAA. The IAA images are obtained by using a uniform angular scanning grid for the azimuth angle ranging from $90°$ to $270°$ with a $2°$ grid size, i.e., $\bar{K}=90$, and also a uniform Doppler scanning grid for the Doppler frequency ranging from $-\pi$ to π with $\bar{K}=256$. Note that the two moving targets are clearly visible both with and without the steering vector errors. In the absence of steering vector errors, the IAA image is close to the clairvoyant image of known $\mathbf{R}_{\mathrm{TCN}}(i)$. In the presence of steering vector errors, the angle-Doppler image formed by IAA is better than the clairvoyant image of known $\mathbf{R}_{\mathrm{TCN}}(i)$, due to the robustness of IAA against steering vector errors. The robustness of IAA is due to the fact that the steering vectors used to form $\mathbf{R}_{\mathrm{IAA}}(i)$ are not the true ones, but the assumed ones and using the same assumed steering vectors with $\mathbf{R}_{\mathrm{IAA}}(i)$ will not result in severe signal cancellation.

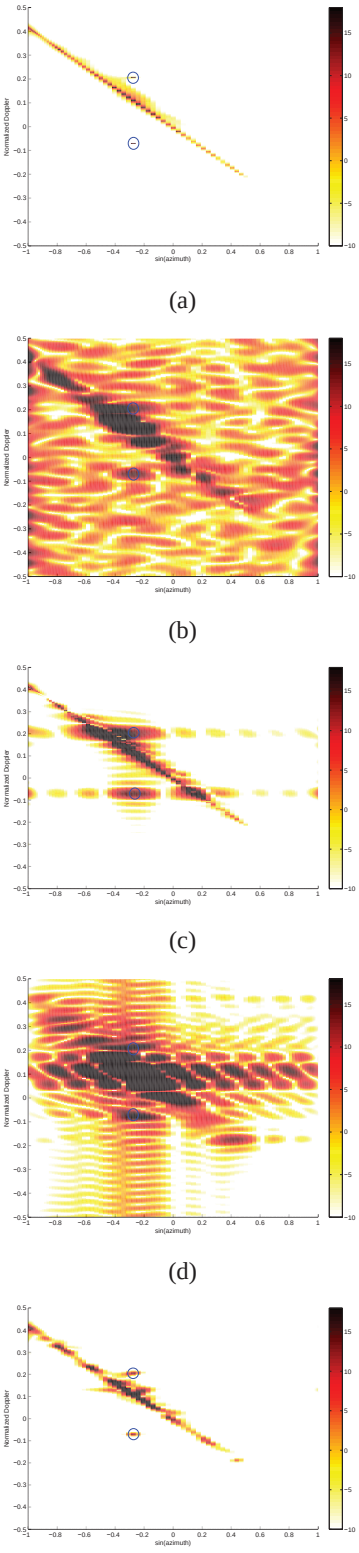

Fig. 2. Angle-Doppler images for the $i = 66$th range bin obtained by using (a) $\mathbf{R}_{\text{TCN}}(i)$, (b) $\mathbf{R}_0(i)$, (c) $\mathbf{R}_{\text{CN}}(i)$, (d) DAS, and (e) IAA, in the absence of steering vector errors. The two circles indicate the true locations of the two moving targets.

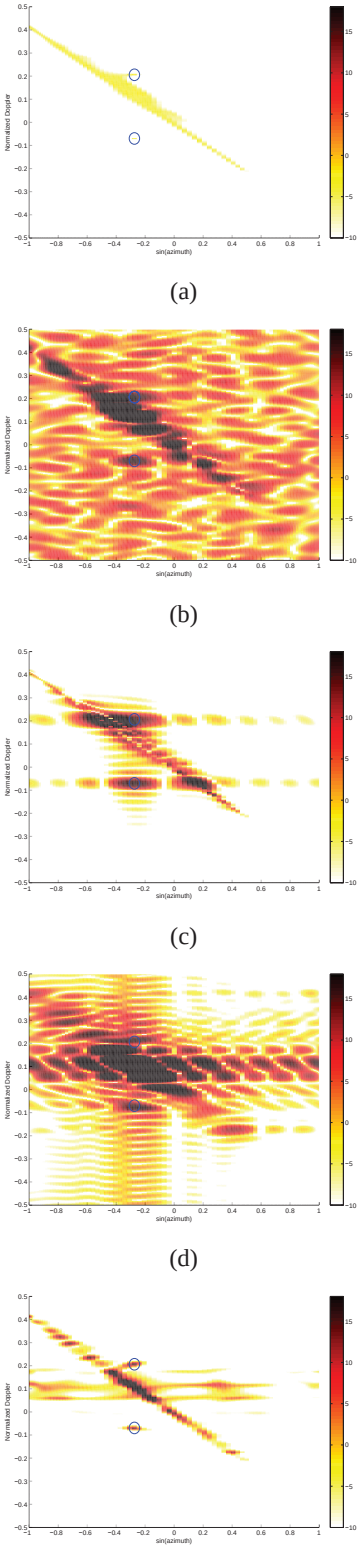

Fig. 3. Angle-Doppler images for the $i = 66$th range bin obtained by using (a) $\mathbf{R}_{\text{TCN}}(i)$, (b) $\mathbf{R}_0(i)$, (c) $\mathbf{R}_{\text{CN}}(i)$, (d) DAS, and (e) IAA, in the presence of steering vector errors. The two circles indicate the true locations of the two moving targets.

3.1.2. Target Detection

Below, we consider using the angle-Doppler images generated by IAA with a simple median detector for target detection. The full potential offered by exploiting the high quality angle-Doppler images formed by IAA can be investigated further. This, however, is beyond the scope of the current paper.

We consider target detection using the angle-Doppler images generated by using the various covariance matrices with ω_{S} fixed to ω_{S_0} corresponding to the 195° azimuth angle. For the range-Doppler image corresponding to a specific range bin, the clutter discretes and the targets will look alike. Therefore, we need a way to distinguish between targets and clutter to avoid false alarms. One might think of discarding the peaks that are close to the diagonal clutter ridge. This would require prior knowledge on operating parameters of the radar, and also there is no clear guidance as to how to determine the "width" of the ridge. Another way, which will be used here, is to rely on the assumption that for the fixed angle and a given Doppler bin, the clutter peaks will be nearly the same in a few (say, 10) range bins that are adjacent to each ROI, whereas the target peaks are not so "dense" in range. We use a median constant false alarm (CFAR) detector, which has the following form [3]:

$$10\log_{10}\left|\frac{\mathbf{a}^*(\omega_{\text{S}},\omega_{\text{D}})\tilde{\mathbf{R}}^{-1}(i)\mathbf{y}_i}{\mathbf{a}^*(\omega_{\text{S}},\omega_{\text{D}})\tilde{\mathbf{R}}^{-1}(i)\mathbf{a}(\omega_{\text{S}},\omega_{\text{D}})}\right|^2 - 10\log_{10}\eta(i,\omega_{\text{S}_0},\omega_{\text{D}}) \underset{\text{H}_0}{\overset{\text{H}_1}{\gtrless}} \xi, \tag{12}$$

where H_0 is the null hypothesis (i.e., no target), H_1 is the alternative hypothesis (i.e., H_0 is false) and ξ is a target detection threshold. The background clutter-and-noise level $\eta(i,\omega_{\text{S}_0},\omega_{\text{D}})$ for range bin i, spatial frequency ω_{S_0}, and Doppler frequency ω_{D} is estimated as the median value of the set of power levels from 10 adjacent range bins at $(\omega_{\text{S}_0},\omega_{\text{D}})$. For each threshold ξ, the number of correct target detections as well as the number of false alarms are recorded to yield the receiver operating characteristic (ROC) [i.e., the probability of detection (PD) versus the probability of false alarm (PFA)] curves. In our simulations, the kth target with Doppler frequency ω_{D_k} is considered to be detected correctly if there are any number of detections in the i_kth range bin falling within the interval $(\omega_{\text{D}_k}-\pi/32,\omega_{\text{D}_k}+\pi/32)$. We remark that the median CFAR detector does not use the data from the adjacent range bins in the same way as the conventional STAP approaches do since the adjacent range bins are used by the detector *after* space-time adaptive processing and are for local comparison of power levels only. The conventional STAP approaches use the secondary data *for* space-time adaptive processing.

In Figure 4, we show the ROC curves of the IAA-based median detector [(12) with $\tilde{\mathbf{R}}(i)$ replaced by $\mathbf{R}_{\text{IAA}}(i)$]. For comparison purposes, we also show the ROC curves corresponding to the detectors with $\mathbf{R}_{\text{TCN}}(i)$ known precisely [(12) with $\tilde{\mathbf{R}}(i)$ replaced by $\mathbf{R}_{\text{TCN}}(i)$], with $\mathbf{R}_{\text{CN}}(i)$ known precisely [(12) with $\tilde{\mathbf{R}}(i)$ replaced by $\mathbf{R}_{\text{CN}}(i)$], and also with $\mathbf{R}_{\text{CN}}(i)$ known imprecisely [(12) with $\tilde{\mathbf{R}}(i)$ replaced by $\mathbf{R}_0(i)$]. Figures 4(a) and 4(b) are for the cases of without and with steering vector errors, respectively. As we can see, in the absence of steering vector errors, the detection performance of using the angle-Doppler images obtained by IAA almost coincides with that of the clairvoyant case where $\mathbf{R}_{\text{TCN}}(i)$ is known precisely. In the presence of steering vector errors, however, using the angle-Doppler images obtained by IAA outperforms even the clairvoyant case of using the precisely known $\mathbf{R}_{\text{TCN}}(i)$. This is not surprising because SCB is sensitive to array steering vector errors whereas IAA is robust against such errors. Note also that using the angle-Doppler images obtained by IAA outperforms the case of using precisely known $\mathbf{R}_{\text{CN}}(i)$ as well.

3.2. KASSPER Data

Finally, we evaluate the performance of IAA using the KASSPER data [12]. In addition to the inhomogeneous clutter (with $\mathbf{R}_{\text{CN}}(i)$ varying with range bin i), the KASSPER data also include many real-world scenarios, such as subspace leakage, array calibration errors (and hence steering vector errors), and many ground targets. Moreover, some of the targets have rather weak power levels and some of them are very slowly moving, which makes the KASSPER data more challenging than our simulated data.

The radar main-beam of the KASSPER data has a width of 10°. The radar attempts to detect targets in the azimuth range of $[190^\circ, 200^\circ]$ instead of a fixed azimuth angle of 195°. Therefore, in addition to range and Doppler, the azimuth angle is treated as another dimension (in our simulated data, we fixed the azimuth angle at 195°). Given the spatial and Doppler frequency pair $(\omega_{\text{S}_k},\omega_{\text{D}_k})$ of the kth target, the target is considered to be detected if there are any number of detections in the i_kth range bin falling within the area of $(\theta_k-5^\circ,\theta_k+5^\circ)$ and $(\omega_{\text{D}_k}-\pi/32,\omega_{\text{D}_k}+\pi/32)$. The corresponding ROC curves are shown in Figure 5. (Note that the target power information used to generate the KASSPER data is not available to us. Therefore, $\mathbf{R}_{\text{TCN}}(i)$ is unknown and the corresponding ROC curve is not shown in Figure 5.) Again, IAA gives the best performance and outperforms even the detector using the perfect prior knowledge of $\mathbf{R}_{\text{CN}}(i)$.

4. CONCLUSIONS

We have presented a nonparametric iterative adaptive approach (IAA) to angle-Doppler imaging for airborne surveillance radar systems. IAA *is robust and user parameter free and it requires no secondary data.* Due to adapting to both clutter and targets, the angle-Doppler images formed via IAA have much higher resolution and much lower sidelobe levels

than conventional approaches. We have used both simulated and KASSPER data to demonstrate the usefulness of using IAA to form high quality angle-Doppler images for STAP applications.

5. REFERENCES

[1] J. Ward, "Space-time adaptive processing for airborne radar," Technical Report 1015, MIT Lincoln Laboratory, December 1994.

[2] J. R. Guerci and E. J. Baranoski, "Knowledge-aided adaptive radar at DARPA," *IEEE Signal Processing Magazine*, pp. 41–50, January 2006.

[3] J. S. Bergin, C. M. Teixeira, P. M. Techau, and J. R. Guerci, "STAP with knowledge-aided data prewhitening," *IEEE Radar Conference, PA*, April 26-28 2004.

[4] P. Stoica, J. Li, X. Zhu, and J. R. Guerci, "On using a priori knowledge in space-time adaptive processing," *IEEE Transactions on Signal Processing*, vol. 56, pp. 2598–2602, June 2008.

[5] H. Wang and L. Cai, "On adaptive spatial-temporal processing for airborne radar systems," *IEEE Transactions on Aerospace and Electronic Systems*, vol. 30, pp. 660–670, July 1994.

[6] T. K. Sarkar, H. Wang, S. Park, R. Adve, J. Koh, K. kim, Y. Zhang, M. C. Wicks, and R. D. Brown, "A deterministic least-squares approach to space-time adaptive processing," *IEEE Transactions on Antennas and Propagation*, vol. 49, pp. 91–103, January 2001.

[7] S. Maria and J. Fuchs, "Application of the global matched filter to stap data: an efficient algorithmic approach," *Proceedings of the IEEE Conference on Acoustic, Speech and Signal Processing*, Toulouse, France, May 2006.

[8] J. R. Roman, M. Rangaswamy, D. W. Davis, Q. Zhang, B. Himed, and J. H. Michels, "Parametric adaptive matched filter for airborne radar applications," *IEEE Transactions on Aerospace and Electronics Systems*, vol. 36, pp. 677–692, April 2000.

[9] K. J. Sohn, H. Li, and B. Himed, "Parametric glrt for multichannel adaptive signal detection," *IEEE Transactions on Signal Processing*, vol. 55, pp. 5351–5360, November 2007.

[10] T. Yardibi, J. Li, P. Stoica, M. Xue, and A. B. Baggeroer, "Source localization and sensing: A nonparametric iterative adaptive approach based on weighted least squares," submitted to *IEEE Transactions on Aerospace and Electronic Systems*, 2007.

[11] M. Wax and T. Kailath, "Efficient inversion of toeplitz-block toeplitz matrix," *IEEE Transactions on Acoustics, Speech, and Signal Processing*, vol. 31, pp. 1218–1221, October 1983.

[12] J. S. Bergin and P. M. Techau, "High-fidelity site-specific radar simulation: KASSPER'02 workshop datacube," *Technical report, Information Systems Laboratories, Inc.*, 2002.

[13] J. Li and P. Stoica, eds., *Robust Adaptive Beamforming*. New York, NY: John Wiley & Sons, 2005.

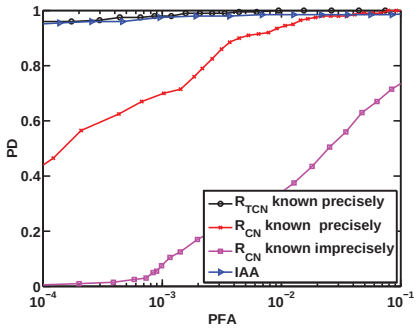

(a)

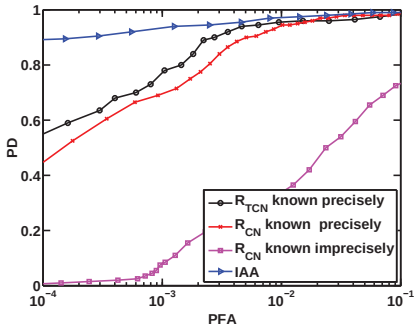

(b)

Fig. 4. ROC curves for our simulated data, generated by using the KASSPER clutter parameters, for the cases of: (a) without steering vector errors, and (b) with steering vectors errors.

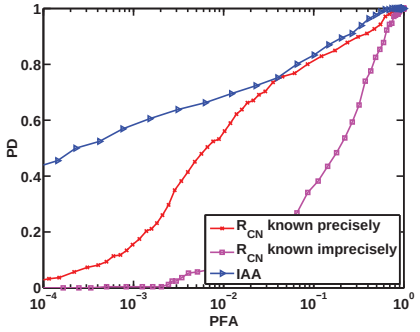

Fig. 5. ROC curves for the KASSPER dataset.